Pure Appl. Chem., Vol. 73, No. 3, pp. 535–542, 2001.

Molecular and biomolecular optoelectronics*

Itamar Willner† and Bilha Willner

Institute of Chemistry, The Farkas Center for Light-Induced Processes, The Hebrew University of Jerusalem, Jerusalem, 91904, Israel

Abstract: Reversible electronic transduction of photonic processes occurring on electrodes is the conceptual method to develop molecular and biomolecular optoelectronic systems. Cyclic photochemical activation of molecular or biomolecular monolayer redox-functions provides a general methodology for the amperometric transduction of photonic information that is recorded by the chemical assembly. Alternatively, photoisomerizable monolayers associated with electrodes act as "command interfaces" for controlling the interfacial electron transfer between molecular redox-species or redox-proteins. The systems use a photonic input for the generation of an electronic output and act as information processing assemblies. Programmed arrays of photosensitizer/electron acceptor cross-linked Au-nanoparticle arrays are assembled on indium tin oxide (ITO) for photoelectrochemical applications.

The miniaturization of devices to molecular or nanoscale dimensions represents a challenging research topic in modern science [1,2]. Photonic activation of electronic functions in nanostructured assemblies may have important implications in designing molecular-based logic gates [3], information storage and processing devices [4], and in the tailoring of new sensors [5], optical switches [6], and solar cells [7].

Several basic features should characterize photoactivated molecular arrays that act as electronic devices: (i) Photoactive molecular or nanoparticle architectures must be integrated with electronic transducers such as electrodes, piezoelectric crystals or field-effect-transistors; (ii) The photonic signal should trigger a chemical or physical function in the nanostructured array. This may include the photonic activation of a binding process [8], molecular translocation [9], redox-functions [10], electron transfer [11], wettability [12], or sol-gel transitions [13]; (iii) The photonic activation of the device functions should be reversible. (iv) The photonically triggered chemical functions in the organized molecular or nanoparticle architectures should be electronically transduced in the form of current, voltage, or other electronic outputs. The present account describes novel methods to organize photoactive molecular [14], biomolecular [15], and nanoparticle arrays [16] on electronic transducers, and addresses the possible applications of these systems as "smart interfaces" for information storage and processing, sensing and the control of the electron-transfer properties at electrodes.

Scheme 1A shows a general scheme for the amperometric transduction of photonic information recorded by a photoisomerizable monolayer-interface associated with the electrode. State A of the monolayer is redox-inactive and does not electronically communicate with the electrode. Photoisomerization of the interface to state B results in a redox-active species, and the recorded optical signal is amperometrically transduced. Irradiation of the redox-active monolayer at another wavelength regenerates the redox-inactive monolayer, and the primary photonic information recorded by the system is erased. Thus, the system describes a "Write-Read-Erase" system. Figure 1A shows the assembly of a photoisomerizable phenoxynaphthacene quinone monolayer-electrode that acts as a photochemical switch according to Scheme 1A [17]. The carboxymethyl phenoxy naphthacene quinone (**1**) was cova-

*Lecture presented at the XVIII[th] IUPAC Symposium on Photochemistry, Dresden, Germany, 22–27 July 2000. Other presentations are published in this issue, pp. 395–548.

†Corresponding author

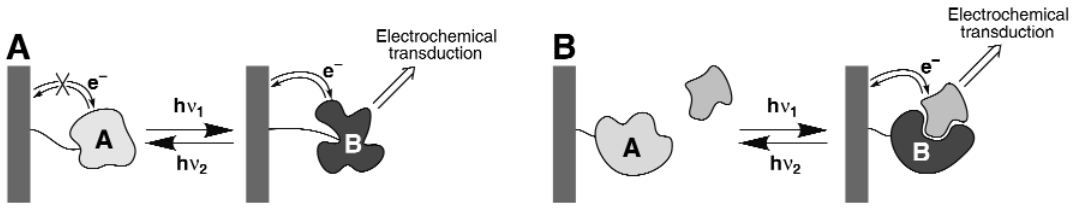

Scheme 1 (A) Amperometric transduction of a redox-activated photoisomerizable interface. (B) Control of the interfacial electron transfer at an electrode functionalized with a "command interface".

lently linked to a cystamine monolayer associated with an Au-electrode. The resulting *trans*-quinone monolayer was structurally rigidified with tetradecanethiol ($C_{14}H_{29}SH$) to yield a densely packed photoisomerizable interface. Figure 1B shows the photoswitchable amperometric transduction of photonic signals recorded by the monolayer. In the *trans*-quinone state, a quasi-reversible redox wave of the quinone units is observed, curve a. Photoisomerization of the monolayer with UV light to "ana" quinone state results in a redox-inactive interface that does not lead to any amperometric response. Visible-light isomerization of the "ana" quinone state to the *trans*-quinone regenerates the redox-active interface, and thus by illumination of the assembly at two distinct wavelength regions, cyclic amperometric transduction of the recorded photonic signals is accomplished, Fig. 1B, inset.

A different approach for the amperometric transduction of recorded photonic signals is schematically shown in Scheme 1B. A photoisomerizable layer associated with the electrode acts as "command interface" for controlling the interfacial electron transfer at the conductive support. In state A of the layer, the electrical communication between the redox-label in solution and the electrode is blocked. Photoisomerization of the layer to state B results in a binding domain for the redox-label. The association of the redox-probe to the photogenerated binding site permits the electrical transduction of the photoisomerization event that occurred on the surface. Thus, the cyclic photoisomerization of the monolayer yields a "command interface" that controls the electrical communication between the redox-probe and the electrode. An assembly that operates according to this concept is depicted in Fig. 2A [11]. A

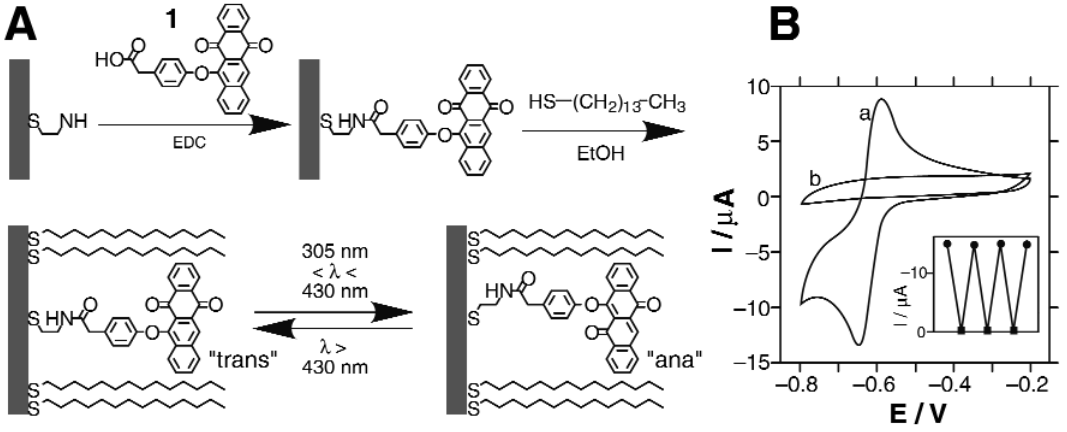

Fig. 1 (A) Assembly of a photoisomerizable phenoxynaphthacene quinone monolayer on an Au-electrode. (B) Cyclic voltammograms of: (a) the "*trans*"-quinone state; (b) the "*ana*"-quinone state. Inset: Cyclic amperometric responses upon the reversible photoisomerization of the monolayer between the "*trans*"-quinone and "*ana*"-quinone states. Data recorded in 0.01 M phosphate buffer and 0.1 M Na_2SO_4, pH = 7.0, scan rate 50 $mV \cdot s^{-1}$.

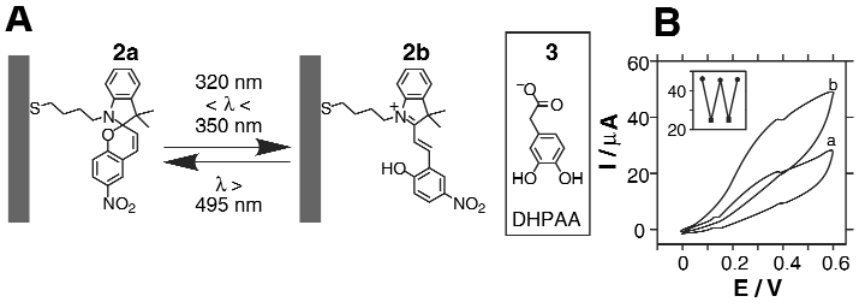

Fig. 2 (A) Assembly of a photoisomerizable nitrospiropyran monolayer on an Au-electrode. (B) Cyclic voltammograms corresponding to the electrochemical oxidation of (**3**) by: (a) The (**2a**)-monolayer-functionalized electrode. (b) The (**2b**)-monolayer-functionalized electrode. Inset: Cyclic switchable oxidation of (**3**) upon the photoisomerization of the monolayer interface between states (**2b**) and (**2a**), respectively. Data recorded in 0.02 M phosphate buffer, pH = 7.0, scan rate 200 $mV \cdot s^{-1}$.

thiolated nitrospiropyran (**2a**) monolayer is assembled on an Au-electrode. UV irradiation of the monolayer-electrode in a phosphate buffer solution, pH = 7.0, yields the positively charged protonated merocyanine interface, (**2b**). Control of the electrical properties of the electrode interface enables photoswitchable redox-processes at the modified electrode, Fig. 2B. The electrooxidation of dihydroxyphenylacetic acid, DHPAA, (**3**), is blocked in the presence of the neutral nitrospiropyran monolayer, while the electrostatic attraction of (**3**) to the protonated nitromerocyanine interface facilitates the electrooxidation of DHPAA, (**3**). By the cyclic photoisomerization of the monolayer between the states (**2a**) and (**2b**) a "command interface" that reversibly switches the electrochemical oxidation of (**3**) between "OFF" and "ON" states, respectively, is generated, Fig. 2B, inset.

The photochemical redox-activation of biomaterials associated with electrodes may further provide means to generate smart interfaces for the electronic transduction of optical information. The evolutionary optimized biocatalytic functions of enzymes or redox-proteins could allow the amplification of the recorded photonic signals through the respective bioelectrocatalytic transformations. The architecture of a light-triggered redox-activated enzyme electrode is described in Scheme 2. The photoswitchable glucose oxidase, GOx, biocatalyst was prepared by the reconstitution method outlined in Scheme 2A. The native FAD-cofactor was extracted from the enzyme, and a semisynthetic photoisomerizable flavin-adenine dinucleotide consisting of nitrospiropyran covalently linked to an amino-FAD, (**4a**), was implanted into the apo-GOx [18]. The resulting photoisomerizable biocatalyst was then

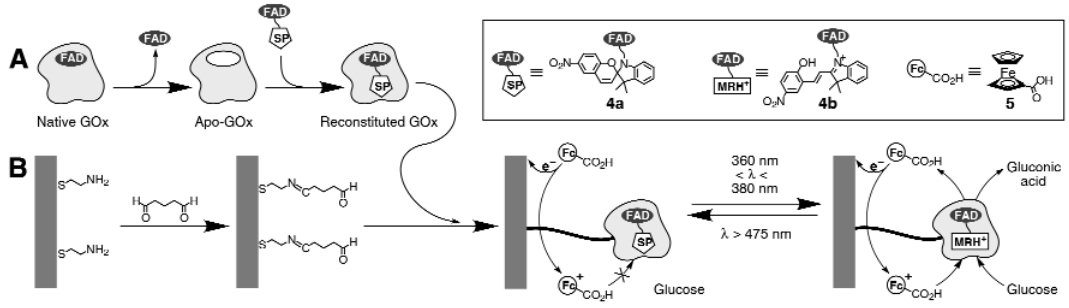

Scheme 2 (A) Reconstitution of apo-glucose oxidase, apo-GOx, with a semisynthetic nitrospiropyran-FAD cofactor. **(B)** The assembly of the reconstituted photoisomerizable glucose oxidase on an Au-electrode and the photoswitchable amperometric transduction of photonic signals recorded by the photoisomerizable enzyme-interface.

assembled as a monolayer on an Au-electrode by the method shown in Scheme 2B. In the presence of ferrocene carboxylic acid, (**5**), as a diffusional electron mediator, the photoswitchable activation of the GOx-functionalized electrode is accomplished, Fig. 3. The nitrospiropyran photoisomer state is redox-inactive towards the oxidation of glucose, Fig. 3, curve a, while photoisomerization of the enzyme interface to the protonated nitromerocyanine-FAD state, (**4b**), activates the bioelectrocatalyzed oxidation of glucose, as evidenced by the electrocatalytic anodic current, Fig. 3, curve b. By the cyclic photoisomerization of the enzyme, the bioelectrocatalyzed oxidation of glucose is reversibly switched between "ON" and "OFF" states, respectively. Mechanistic studies indicate that the neutral nitrospiropyran photoisomer state blocks the penetration of (**5**) into the protein, thus perturbing the electrical contacting of the FAD-redox-center with the electrode. Photoisomerization of the enzyme layer to the protonated dinitromerocyanine configuration opens an intraprotein channel for the mediated electron transfer and the activation of the enzyme for the bioelectrocatalyzed oxidation of glucose. The biocatalyzed oxidation of glucose provides an amplification path for the amperometric transduction of the molecular photoisomerization event.

The amperometric transduction of recorded photonic information by the integration of biomaterials with a photo-command interface [19], is shown in Fig. 4A. A mixed monolayer consisting of mercaptopyridine and nitrospiropyran photoisomerizable units (ratio 1:10) is assembled on an Au-electrode. The pyridine units act as binding sites for the association of the hemoprotein cytochrome c, Cyt. c, on the conducting support. The binding of Cyt. c to the pyridine sites results in the alignment of the hemoprotein and its electrical contacting with the electrode. Photoisomerization of the monolayer to the protonated nitromerocyanine configuration results in the electrostatic repulsion of the positively charged Cyt. c and its dissociation from the electrode support. Dissociation of the pyridine-Cyt. c complex blocks the electrical communication between the hemoprotein and the electrode. Figure 4B shows the cyclic amperometric transduction of the photonic signals that cause the isomerization of the monolayer, and the reversible binding and dissociation of Cyt. c to and from the photoisomerizable interface, respectively.

Tailoring of nanostructured photoelectrochemical systems is another challenging facet of molecular optoelectronics. We describe here the construction of layered arrays consisting of nanoparticles cross-linked by molecular functionalities and discuss the chemical, physical, and electronic functions of these assemblies. Specifically, we address cooperative effects in the photoactive molecular-cross-

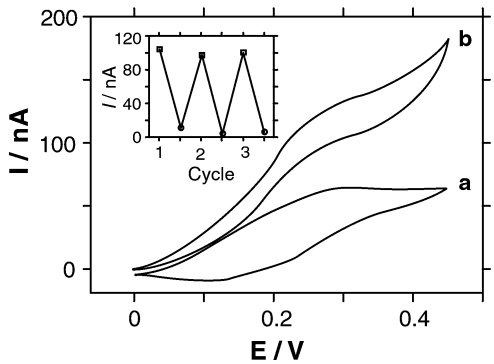

Fig. 3 Cyclic voltammograms corresponding to the photoswitchable bioelectrocatalyzed oxidation of glucose, 5×10^{-2} M, by the photoisomerizable glucose oxidase monolayer-electrode: (a) Nitrospiropyran-FAD enzyme state. (b) Protonated nitromerocyanine-FAD enzyme state. Inset: Cyclic amperometric transduction of the photonic signals recorded by the photoisomerizable glucose oxidase-monolayer-electrode. Data recorded in 0.01 M phosphate buffer, and 0.1 M Na_2SO_4, pH = 7.3, scan rate 5 $mV \cdot s^{-1}$, in the presence of (**5**), 5×10^{-5} M.

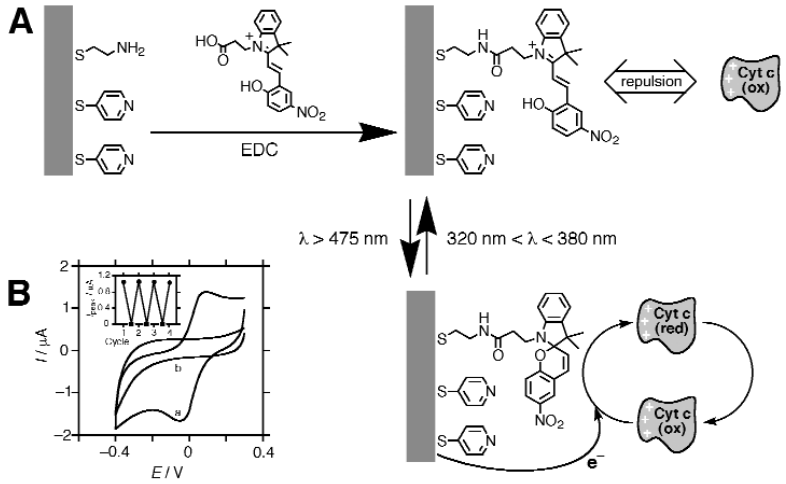

Fig. 4 (A) Assembly of a thiol pyridine/nitrospiropyran mixed monolayer on an Au-electrode acting as a "command interface" for controlling the interfacial electron transfer to cytochrome c. (B) Photoswitchable electrical contacting of Cyt. c with the photoisomerizable monolayer-functionalized electrode: (a) Monolayer in the pyridine/nitrospiropyran state. (b) Monolayer in the pyridine/protonated nitromerocyanine state. Inset: Cyclic electrical contacting of Cyt. c with the electrode upon the reversible photoisomerization of the mixed monolayer between states. Cyclic voltammograms were recorded in 0.01 M phosphate buffer, pH = 7.2, scan rate 50 $mV \cdot s^{-1}$.

linked nanoparticle arrays that lead to unique photoelectrochemical and sensoric functions. In a series of studies we demonstrated the construction of layered Au-nanoparticle arrays by cross-linking of negatively charged citrate-capped Au-nanoparticles with oligocationic molecular cross-linkers [20,21]. By the stepwise deposition of cross-linked Au-nanoparticles on conductive surface, arrays of controlled thickness, exhibiting three-dimensional conductivity, were generated. This method was applied for the assembly of nanostructured electrodes for photoelectrochemical applications, Scheme 3 [22,23]. An aminosiloxane-functionalized ITO-electrode acts as the base surface for the assembly of the first layer of Au-nanoparticles. By the stepwise association of the positively charged photosensitizer-electron acceptor dyads, e.g., the Zn(II)-protoporphyrin IX-*bis*-bipyridinium, (**6**), or the Ru(II)-*tris*-bipyridine-*bis*-phenylene (paraquat)-catenane, (**7**), and then the binding of Au-nanoparticles, an array with a controlled number of cross-linked nanoparticles is generated.

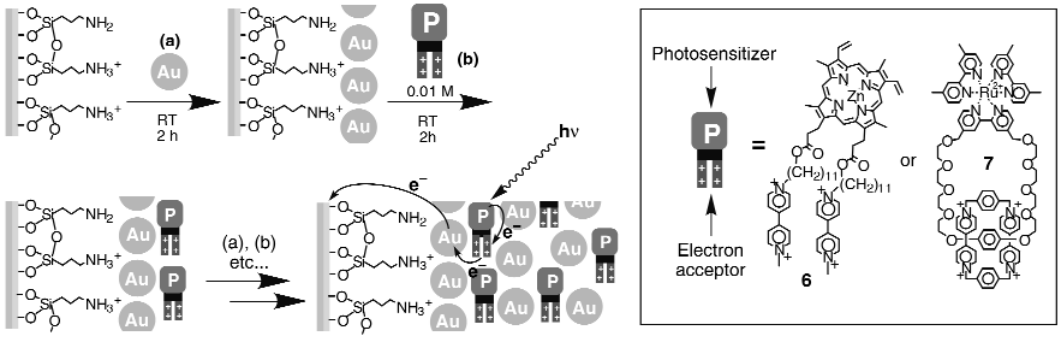

Scheme 3 Assembly of layered photosensitizer-electron-acceptor-cross-linked Au-nanoparticle arrays on an electrode for photoelectrochemical applications.

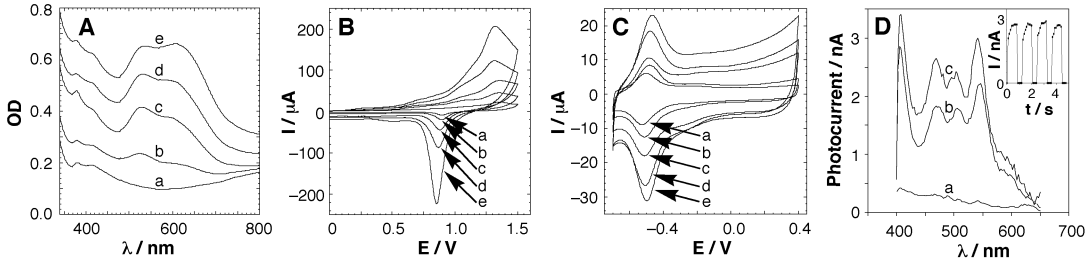

Fig. 5 Characterization and photoelectrochemical functions of the layered (**6**)-cross-linked Au-nanoparticle arrays. **(**A**)** Absorbance spectra of the (**6**)-cross-linked Au-nanoparticle arrays, (a) to (e) one to five Au-nanoparticle layers. **(**B**)** Cyclic voltammograms of the Au-nanoparticle layers in 1 M H_2SO_4, (a) to (e) one to five Au-nanoparticle layers, scan rate 50 $mV \cdot s^{-1}$. **(**C**)** Cyclic voltammograms of the (**6**)-cross-linked Au-nanoparticle layers in 0.1 M phosphate buffer, pH = 7.2, (a) to (e) one to five layers, scan rate 100 $mV \cdot s^{-1}$. **(**D**)** Photocurrent action spectra upon irradiation of: (a) A monolayer of bare Au-nanoparticles. (b) One layer of Au-nanoparticles with associated (**6**). (c) Three layers of (**6**)-cross-linked Au-nanoparticles. Inset: Cyclic switchable photocurrents upon the pulsed irradiation, λ = 544 nm, of a three-layer (**6**)-cross-linked Au-nanoparticle array.

Figure 5 shows the methods that were employed to characterize the array of (**6**)-cross-linked Au-nanoparticles and the photocurrent generated by the nanostructured electrode. Figure 5A shows the absorbance spectra observed upon the build-up of the array. The increase of the characteristic plasmon absorbance of Au-nanoparticles, λ = 520 nm, with the concomitant increase of an interparticle coupled plasmon absorbance at λ = 620 nm for higher degrees of aggregation is observed. Figure 5B shows the voltammetric waves corresponding to the bipyridinium cross-linking units, upon the construction of the Au-nanoparticle layers. An almost linear increase in the electrochemical response is detected, implying that the 3D-array is conductive. Figure 5C shows the redox response of the Au-nanoparticles in 1 M H_2SO_4 upon the construction of the layers. The gradual increase in the Au-nanoparticle response confirms the construction of the aggregated array. By coulometric assay of the electrical response of the bipyridinium units and of the Au-nanoparticle waves, and knowing the size of the Au-particle, we estimate that ca. 260-chromophore-electron-acceptor units are associated with each Au-nanoparticle. Figure 5D shows the photocurrent action spectra of the array as a function of the number of Au-nanoparticle layers. The photocurrent spectra match the absorption spectrum of the Zn(II)-porphyrin chromophore. The photocurrent is blocked upon biasing the electrode potentials at values that are more negative than the redox-potential of the bipyridinium units. This implies that the photocurrent originates from the intramolecular electron transfer quenching of the chromophore by the bipyridinium units, followed by the tunneling of the electrons to the electrode by the conductive array of Au-nanoparticles.

The molecular cross-linking of nanoparticle arrays on electrode supports was further employed to generate DNA-cross-linked CdS-nanoparticles for photoelectrochemical applications, Scheme 4 [24]. The system provides a novel optobioelectronic assembly for the optical and photoelectrochemical detection of DNA. An oligonucleotide primer, (**8**), that is partially complementary to the analyte DNA, (**9**), is assembled on glass or conductive ITO supports. Upon interaction of the (**8**)-functionalized surfaces with the analyte DNA, (**9**), and then with CdS-nanoparticles functionalized with the oligonucleotide (**10**), being complementary to the other part of the analyte DNA, the first layer of CdS-nanoparticles is generated on the surface. By the subsequent treatment of the CdS-nanoparticle layer with the analyte (**9**) and CdS-nanoparticles, functionalized alternatively by (**8**) or (**10**), a cross-linked array of CdS-nanoparticles of controlled aggregation is generated. The action spectra of the photocurrents developed in the systems follow the absorption spectrum of the CdS-nanoparticles. The photocurrents are enhanced as the number of layers of the CdS-nanoparticles increases.

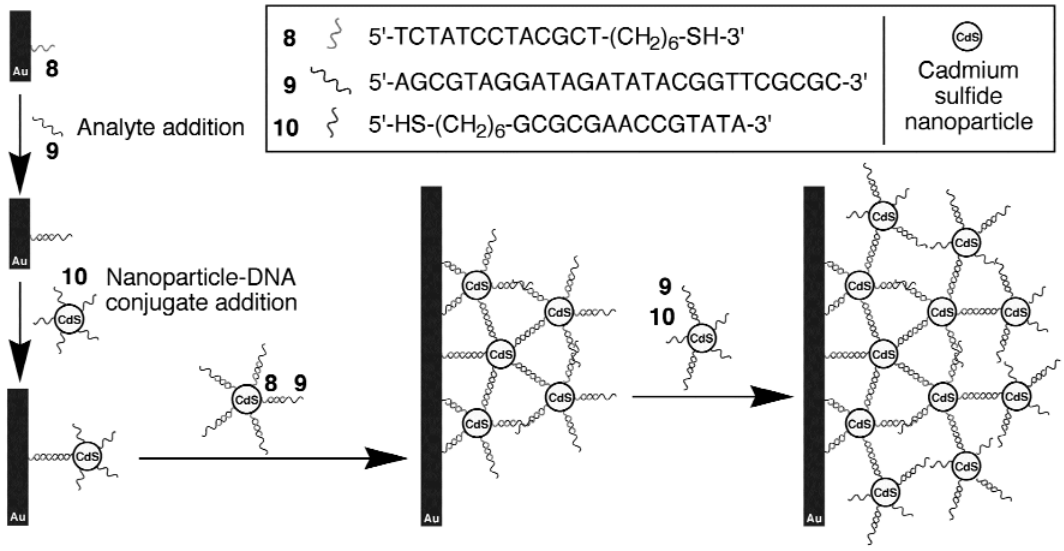

Scheme 4 Assembly of a double-stranded oligonucleotide-DNA-cross-linked CdS-nanoparticle array of controlled aggregation for photoelectrochemical sensoric applications.

In conclusion, we demonstrate novel methods for the assembly of photoactive molecular, biomolecular, and nanoparticle architectures on surfaces for optoelectronic applications. Cyclic photonic activation of redox functions of molecular and biomolecular assemblies on electrodes, resulting in the electronic transduction of the recorded optical signals, was employed as a concept to develop optoelectronic information storage and processing devices. The light-induced generation of photocurrents in cross-linked nanoparticle arrays demonstrates novel nanostructures for photoelectrochemical applications, and specifically highlights the integration of DNA and CdS-nanoparticles as new DNA-sensing assemblies.

ACKNOWLEDGMENTS

Parts of this research project were supported by the Israel Science Foundation and the U.S.-Israel Binational Science Foundation.

REFERENCES

1. (a) J.-M. Lehn. *Angew. Chem., Int. Ed. Engl.* **29**, 1304 (1990); (b) F. L. Carter, A. Schultz, D. Duckworth. In *Molecular Electronic Devices*, F. L. Carter (Ed.), p. 183. Marcel Dekker, New York (1987).
2. (a) *Molecular Electronic Devices*, F. L. Carter, R. E. Siatkowsky, H. Woltjien (Eds.), Elsevier, Amsterdam (1988); (b) P. Ball. *Nature* **362**, 123 (1993).
3. A. P. DeSilva, H. Q. N. Gunaratne, C. P. McCoy. *Nature* **364**, 42 (1993).
4. (a) P. Ball and L. Garwin. *Nature* **355**, 761 (1992); (b) D. Bradley. *Science* **259**, 890 (1993).
5. (a) R. A. Bissell, A. P. DeSilva, H. Q. N. Gunaratne, P. L. M. Lynch, G. E. M. Maguire, C. P. McCoy, K. R. A. S. Sandanayake. *Top. Curr. Chem.* **168**, 223 (1993); (b) M. Lahav, E. Katz, A. Doron, F. Patolsky, I. Willner. *J. Am. Chem. Soc.* **121**, 862 (1999); (c) A. B. Kharitonov, A. N. Shipway, I. Willner. *Anal. Chem.* **71**, 5441 (1999).

6. I. Willner and B. Willner. *J. Mater. Chem.* **8**, 2543 (1998).
7. B. O'Regan and M. Grätzel. *Nature* **353**, 737 (1991).
8. (a) F. Würthner and J. Rebek, Jr. *Angew. Chem., Int. Ed. Engl.* **34**, 446 (1995); (b) I. Willner, S. Marx, Y. Eichen. *Angew. Chem., Int. Ed. Engl.* **31**, 1243 (1992); (c) S. Shinkai and O. Manabe. *Top. Curr. Chem.* **121**, 67 (1984).
9. (a) R. A. Bissell, E. Cordova, A. E. Kaifer, J. F. Stoddart. *Nature* **369**, 133 (1994); (b) D. Philp and J. F. Stoddart. *Synlett* 445 (1991); (c) A. C. Benniston, A. Harriman, V. M. Lynch. *J. Am. Chem. Soc.* **117**, 5275 (1995).
10. (a) J. Daub, J. Salbeck, T. Knöchel, C. Fischer, H. Kunkely, K. M. Rapp. *Angew. Chem., Int. Ed. Engl.* **28**, 1494 (1989); (b) J. Daub, C. Fischer, J. Salbeck, K. Ulrich. *Adv. Mater.* **2**, 366 (1990).
11. A. Doron, E. Katz, G. Tao, I. Willner. *Langmuir* **13**, 1783 (1997).
12. M. O. Wolf and M. A. Fox. *J. Am. Chem. Soc.* **117**, 1845 (1995).
13. (a) T. Seki, M. Sakuragi, Y. Kawanishi, Y. Suzuki, T. Tamaki, R. Fukuda, K. Ichimura. *Langmuir* **9**, 211 (1993); (b) K. Aoki, T. Seki, Y. Suzuki, T. Tamaki, A. Hosoki, K. Ichimura. *Langmuir* **8**, 1007 (1992); (c) A. Suzuki and T. Tanaka. *Nature* **346**, 345 (1990). (d) T. Amiya and T. Tanaka. *Macromolecules* **20**, 1162 (1987).
14. I. Willner and B. Willner. *Adv. Mater.* **9**, 351 (1997).
15. (a) I. Willner and S. Rubin. *Angew. Chem., Int. Ed. Engl.* **35**, 367 (1996); (b) I. Willner. *Acc. Chem. Res.* **30**, 347 (1997).
16. A. N. Shipway, E. Katz, I. Willner. *ChemPhysChem* (2000). **1**, 18 (2000).
17. (a) A. Doron, E. Katz, M. Portnoy, I. Willner. *Angew. Chem., Int. Ed. Engl.* **35**, 1535 (1996); (b) A. Doron, M. Portnoy, M. Lion-Dagan, E. Katz, I. Willner. *J. Am. Chem. Soc.* **118**, 8937 (1996).
18. R. Blonder, I. Willner, A. F. Bückmann. *J. Am. Chem. Soc.* **120**, 9335 (1998).
19. M. Lion-Dagan, E. Katz, I. Willner. *J. Chem. Soc., Chem. Commun.* 2741 (1994).
20. (a) A. N. Shipway, M. Lahav, R. Blonder, I. Willner. *Chem. Mater.* **11**, 13 (1999); (b) M. Lahav, A. N. Shipway, I. Willner, M. B. Nielsen, J. F. Stoddart. *J. Electroanal. Chem.* **482**, 217 (2000).
21. M. Lahav, A. N. Shipway, I. Willner. *J. Chem. Soc., Perkin Trans. 2* 1925 (1999).
22. M. Lahav, T. Gabriel, A. N. Shipway, I. Willner. *J. Am. Chem. Soc.* **121**, 258 (1999).
23. M. Lahav, V. Heleg-Shabtai, J. Wasserman, E. Katz, I. Willner, H. Dürr, Y.-Z. Hu, S. Bossmann. J. Am. Chem. Soc. **122**, 15480 (2000).
24. I. Willner, F. Patolsky, J. Wasserman. *Angew. Chem., Int. Ed. Engl.* **40**, 1861 (2001).